

Impact of ROI Size on the Accuracy of Noise Measurement in CT on Computational and ACR Phantoms

Choirul Anam^{1*}, Pandji Triadyaksa¹, Ariij Naufal², Zaenal Arifin², Zaenul Muhlisin², Evi Setiawati², Wahyu Setia Budi¹

ABSTRACT

Background: The effect of region of interest (ROI) size variation on producing accurate noise levels is not yet studied.

Objective: This study aimed to evaluate the influence of ROI sizes on the accuracy of noise measurement in computed tomography (CT) by using images of a computational and American College of Radiology (ACR) phantoms.

Material and Methods: In this experimental study, two phantoms were used, including computational and ACR phantoms. A computational phantom was developed by using Matlab R215a software (Mathworks Inc., Natick, MA Natick, MA) with a homogeneously +100 Hounsfield Unit (HU) value and an added-Gaussian noise with various levels of 5, 10, 25, 50, 75, and 100 HU. The ACR phantom was scanned with a Philips MX-16 slice CT scanner in different slice thicknesses of 1.5, 3, 5, and 7 mm to obtain noise variation. Noise measurement was conducted at the center of the phantom images and four locations close to the edge of the phantom images using different ROI sizes from 3×3 to 41×41 pixels, with an increased size of 2×2 pixels.

Results: The use of a minimum ROI size of 21×21 pixels shows noise in the range of ±5% ground truth noise. The measured noise increases above the ±5% range if the used ROI is smaller than 21×21 pixels.

Conclusion: A minimum acceptable ROI size is required to maintain the accuracy of noise measurement with a size of 21×21 pixels.

Citation: Anam Ch, Triadyaksa P, Naufal A, Arifin Z, Muhlisin Z, Setiawati E, Budi WS. Impact of ROI size on the Accuracy of Noise Measurement in CT on Computational and ACR Phantoms. *J Biomed Phys Eng.* 2022;12(4):359-368. doi: 10.31661/jbpe.v0i0.2202-1457.

Keywords

ACR Phantom; Computational Phantom; Diagnostic Imaging; Image Quality; Noise Measurement; Radiologic Phantoms; Tomography, X-Ray Computed; X-Rays

Introduction

Noise is considered a key factor in evaluating the performance of computed tomography (CT) image quality [1-3]. In addition to noise, other effective factors on the image quality are spatial resolution [4-6] and low-contrast detectability (LCD) [7]. Smaller image noise leads to better image quality [8]. Recent studies have reported that noise affects the accuracies of image spatial resolution and LCD measurements [9-12].

Noise sources are classified into three main categories: image generation process, system limitation, and quantum noise [13]. Several input

¹PhD, Department of Physics, Faculty of Sciences and Mathematics, Diponegoro University, Jl. Prof. Soedarto SH, Tembalang, Semarang 50275, Central Java, Indonesia

²MSc, Department of Physics, Faculty of Sciences and Mathematics, Diponegoro University, Jl. Prof. Soedarto SH, Tembalang, Semarang 50275, Central Java, Indonesia

*Corresponding author: Choirul Anam

Department of Physics, Faculty of Sciences and Mathematics, Diponegoro University, Jl. Prof. Soedarto SH, Tembalang, Semarang 50275, Central Java, Indonesia

E-mail: anam@fisika.fsm.undip.ac.id

Received: 9 February 2022

Accepted: 15 March 2022

parameters affecting the quantum noise are tube current, tube voltage, scan speed, slice thickness, pitch, and filter thickness [13, 14]. Noise as a result of system limitation is considered a form of electronic noise on the detector, the data acquisition system, and scattered radiation [15]. Noise in the image processing is derived from the reconstruction of the algorithm and its parameters, and calibration effectiveness [16-18].

The noise level is generally characterized by the standard deviation (SD) of pixel values in a region of interest (ROI) placed in a homogeneous region [19-21]. For quality control (QC), noise is usually measured on a standardized homogeneous phantom, such as the American College of Radiology (ACR) CT accreditation phantom [22], Catphan phantom [23], and others [24]. However, noise characterization by using its image SD can only determine the amount of noise level, not the type of noise or image texture. The noise power spectrum (NPS) is used to determine the image texture [25-27].

To the best of our knowledge, the effect of the ROI size variation on producing accurate noise level is not yet studied. A specific ROI size in CT image is required to avoid the fluctuations in pixel's Hounsfield unit (HU) values due to the quantum noise effect. Too small ROI size cannot capture all HU fluctuation in the ROI that represents the general image noise. On the contrary, too large the ROI size may capture the fluctuation in pixel values due to factors other than noise, such as the beam hardening phenomenon. The American Association of Physicists in Medicine (AAPM) has reported that ROI size to calculate noise must be at least around 1 cm² [28]. While recently, in 2019, the AAPM reported that the ROI size used to calculate noise is cultivated at around 1% of the image size [29]. Therefore, the evaluation of ROI size in calculating noise is important. This study aimed to evaluate the effect of different ROI sizes on measuring noise at different noise levels by using a

computational phantom with ground truth of noises and images of ACR phantom.

Material and Methods

In this experimental study, two phantoms were used, such as computational and ACR phantoms.

a. Computational phantom

Figure 1a shows the design of the computational phantom constructed using Matlab software with a pixel size of 512×512 in a circular-shaped and a pixel value of +100 HU. The phantom was surrounded by an air background with a value of -1000 HU. The computational phantom, $P(x, y)$, was blended with a point spread function, $PSF(x, y)$, which has the SD value of 1 pixel to imitate the real image from the CT system. The blurring process was conducted by convoluting the phantom image with a point spread function (PSF) [30]. The degradation of the image spatial resolution, $I(x, y)$, was modeled by the equation (1, 2) as follows:

$$I(x, y) = \frac{1}{k} [P(x, y) \otimes PSF(x, y)] \quad (1)$$

Image normalization due to the convolution process was accomplished by dividing the image with k .

$$k = \sum \sum PSF(x, y) \quad (2)$$

Figure 1b presents the degradation result of the phantom image by PSF, i.e. the boundary of the object is not as sharp as the original image of the phantom (Figure 1a). After that, the Gaussian noises were added to the phantom with specific SD, $N(x, y)$ [31], which this Gaussian noise standard deviation was called the ground truth noise. In this study, the added Gaussian noise varies with the SD of 5, 10, 25, 50, 75, and 100 HU. A histogram curve evaluation was conducted to ensure the generation of Gaussian noise at different noise levels. Therefore, a relatively wide ROI of 320×320 pixels, containing 102,400 pixels (Figure 1d)

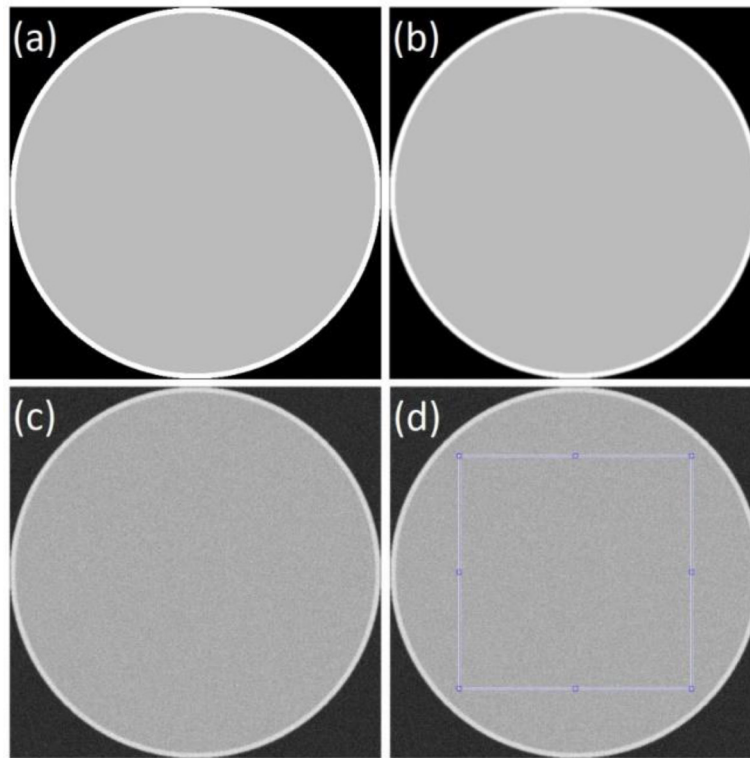


Figure 1: The design of a computational phantom: (a) the phantom has a circle shape with a pixel value of +100 Hounsfield unit (HU) and a pixel number of 512×512 . (b) The quality of phantom images was degraded by using a point spread function (PSF) to decrease the image spatial resolution. (c) The phantom image quality was then degraded again by adding Gaussian noises. (d) For the given Gaussian noise, a square homogeneous area of 320×320 pixels is created to perform a histogram curve evaluation of the pixel's values

was used to perform the evaluation.

b. ACR phantom

The real CT images of the ACR phantom (Gammex Inc., USA) were utilized to evaluate the impact of different ROI sizes on the noise. The ACR phantom consisted of four independent modules to check several parameters of the image separately. For this study, only one module was used, i.e. the distance module. The distance module consisted of a uniform water material (approximately 0 HU) with two very small cube's radiopaque steel balls (called BeeBee (BB)) of ~ 0.28 mm each. The uniform water was usually used to assess the accuracy of CT number of water, CT number uniformity, noise, and noise uniformity, and two BBs were usually used to access dis-

tance accuracy and modulation transfer function (MTF). The phantom was scanned with a Philips MX-16 slice CT scanner. The phantom was scanned with different slice thicknesses of 1.5, 3, 5, and 7 mm to obtain noise variation. Other acquisition parameters were tabulated in Table 1. Images of the distance module scanned with different slice thicknesses were depicted in Figure 2.

c. Noise measurement

The noise was computed at five different ROI locations in the phantoms. The first ROI was located at the center and four were located close to the edge of the phantoms as shown in Figure 3. The center ROI position was located at x, y position of 256, 256, respectively, and the other four ROIs were located on the

right (x, y of 384, 256, respectively), below (x, y of 256, 384, respectively), on the left (x, y of 128, 256, respectively), and top (x, y of 256, 128, respectively) of the phantom. From these five ROIs, the average noise value was

Table 1: Acquisition parameters of computed tomography (CT) scanner to find the images of the American College of Radiology (ACR) phantom.

| Acquisition parameter | Value |
|-------------------------|--------------------------------|
| Tube voltage | 120 kV |
| Tube current | 300 mA |
| Revolution time | 1 s |
| Mode | Helical |
| Pitch | 0.6713 |
| Reconstruction type | Filtered-back Projection (FBP) |
| Reconstruction diameter | 22.2 cm |
| Gantry tilt | 0 degree |
| Slice thicknesses | 1.5, 3, 5, and 7 cm |

acquired, and the SD of noise was calculated. The SD of the pixel value in the ROI placed in a homogeneous area was calculated by the equation (3, 4):

$$\sigma = \sqrt{\frac{\sum_{i,j \in ROI} (I_{i,j} - \bar{I})^2}{N}} \quad (3)$$

with

$$\bar{I} = \frac{1}{N} \sum_{i,j \in ROI} I_{i,j} \quad (4)$$

where N was $n \times n$, which was the number of pixels in ROI. In this study, the size of the ROI was varied from 3×3 to 41×41 pixels with a 2×2 pixels increment as shown in Figure 3.

Results

a. Computational phantom

The histogram evaluation showed that the noise in the computational phantom image

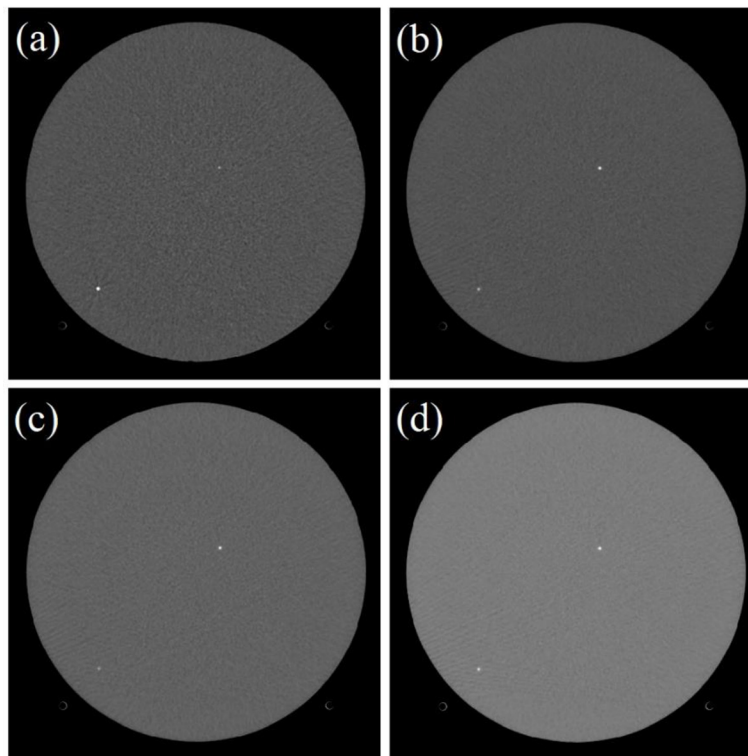


Figure 2: Images of the American College of Radiology (ACR) phantom scanned with various slice thicknesses of (a) 1.5 mm, (b) 3 mm, (c) 5 mm, and (d) 7 mm.

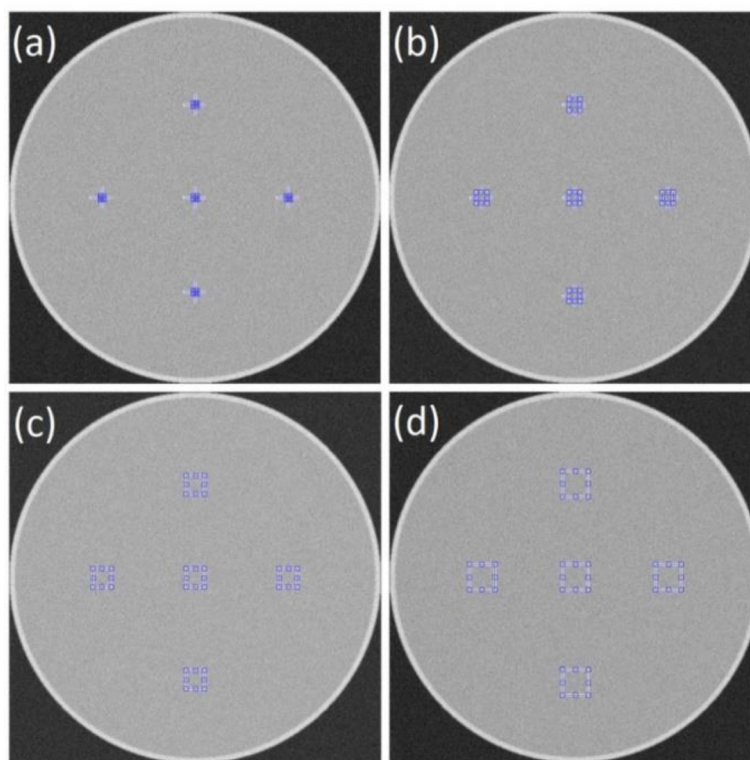


Figure 3: The location of five regions of interest (ROIs) in the phantom. The ROIs have a square size and varied from 3×3 to 41×41 pixels with examples of (a) 5×5 pixels, (b) 15×15 pixels, (c) 25×25 pixels, and (d) 35×35 pixels.

is randomly Gaussian noise with its center (highest frequency) at +100 HU as shown in Figure 4. The x-axis of the histogram is the pixel value, and the y-axis is the frequency of occurrence of pixel values. The number of bins on the x-axis is 50. In Figure 4, the given noise level determines the width of the histogram. Given noise of 5 HU, the SD of the histogram curve is around 5 HU (Figure 4a).

The noise measurements at different ROI sizes are shown in Figure 5; these solid red line shows the value of the given ground truth noise level, and the red dashed line on the graph represents the noise range of $\pm 5\%$ of the ground truth. The use of a smaller ROI size gives less accurate noise measurement with a higher noise SD while using a larger ROI size, more accurate noise measurement, proved by lower noise SD, is produced as close as the given ground truth values. A con-

servative minimum ROI size of 21×21 pixels produces an acceptable noise measurement close to the given ground truth noise with its SD in the range of $\pm 5\%$ from all ground truth values. While by measuring noise using ROI sizes smaller than 21×21 pixels, the measured noises had SD greater than the $\pm 5\%$ noise variation from its ground-truth value reflecting a misleading noise result.

b. ACR phantom

The noise measurements from the ACR phantom images at different ROI sizes for four-slice thicknesses are shown in Figure 6. The noises decrease with the increase of slice thickness, and the noise levels are 8.25, 5, 3.9, 4.64, and 3.34 HU for slice thicknesses of 1.5, 3, 5, and 7 cm, respectively. The red dashed line on the graph of Figure 6 represents the range of $\pm 5\%$ of the average three noises at

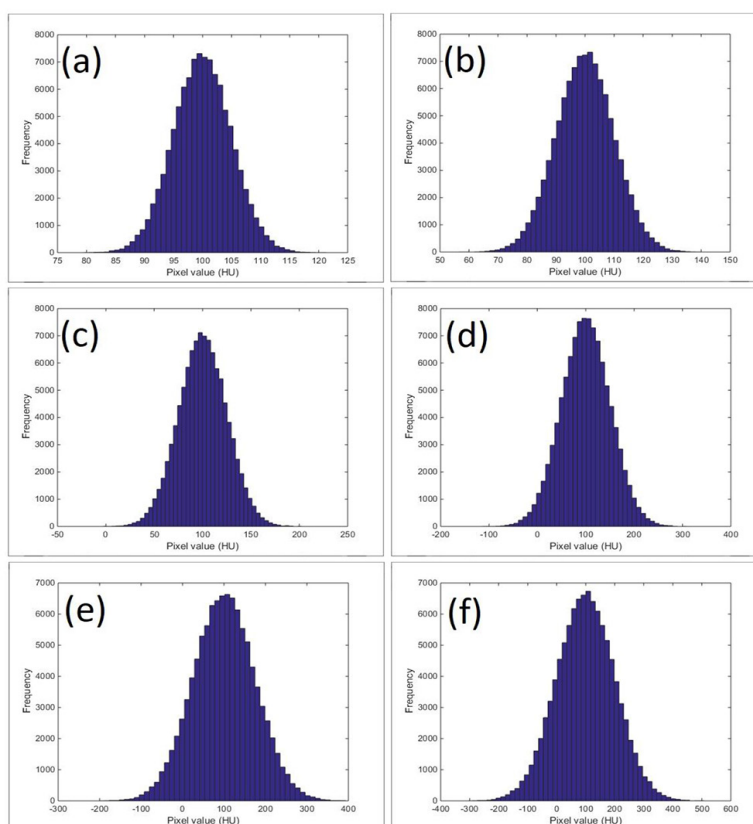


Figure 4: Histograms for several noise levels, (a) 5 Hounsfield unit (HU), (b) 10 HU, (c) 25 HU, (d) 50 HU, (e) 75 HU, and (f) 100 HU, show the noise histogram is in the shape of Gaussian. The peak of the histogram is at a pixel value of +100 HU, which is the pixel value of the phantom, showing the widths of the Gaussian correspond to the given noise levels.

ROI sizes of 37, 39, and 41 pixels. As previously, the use of a small ROI size gives less accurate noise measurement, while using a larger ROI size, more accurate noise measurement is obtained. As previously, a minimum ROI size of 21×21 pixels produces a stable noise in the range of $\pm 5\%$.

Discussion

This study aimed to evaluate the effect of different ROI sizes on measuring noise and investigate the effect at the different noise levels. Two phantoms were utilized, such as computational phantom and the ACR phantom. Several levels of Gaussian noises were applied to the computational phantom, including 5, 10, 25, 50, 75, and 100 HU with its noise distribution obtained by a histogram curve evalu-

ation [32]. Comparing a measured noise with a ground truth noise is a very difficult task in real CT images due to the inability to acquire the ground-truth value. Therefore, many studies on noise evaluation generally only performed the noise pattern, for example, in the relationship between dose and noise [33], in the relationship between tube current type and noise [12], or the relationship between filter type and noise [12,34]. In this study, a computational homogeneous phantom was made by adding a known Gaussian noise in the phantom to acquire a ground truth noise.

In a specific task, an evaluation of noise accuracy using computational phantom images was more objective than using real images due to several reasons as follows: (a) the homogeneity of the object could be guaranteed,

Impact of ROI Size on Accuracy of the Noise Measurement

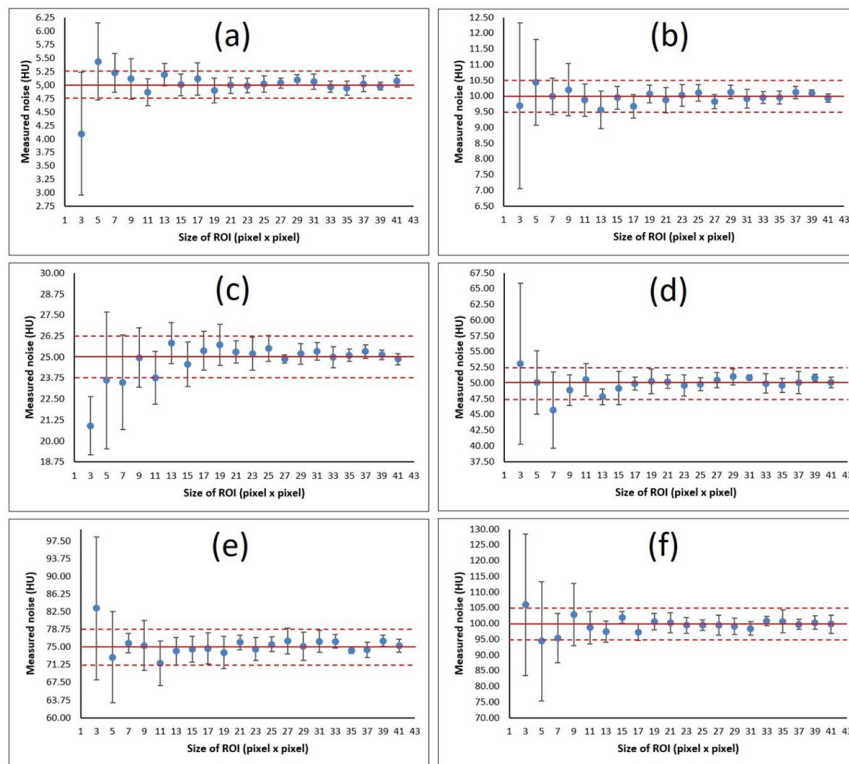


Figure 5: Relationships between measured noises with the sizes of the region of interest (ROI) on some ground truth noises, (a) 5 Hounsfield unit (HU), (b) 10 HU, (c) 25 HU, (d) 50 HU, (e) 75 HU, and (f) 100 HU. The dashed line is the range of $\pm 5\%$ of the ground truth.

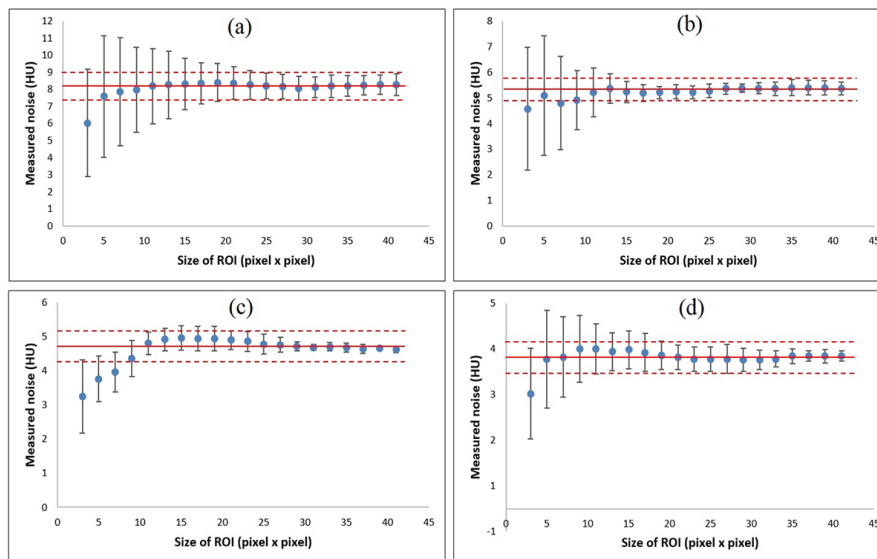


Figure 6: Relationships between measured noises and the sizes of the region of interests (ROIs) on images of American College of Radiology (ACR) phantom for various slice thicknesses, (a) 1.5 mm, (b) 3 mm, (c) 5 mm, and (d) 7 mm. The dashed line is the range of $\pm 5\%$ of the average three noises at ROI sizes of 37, 39, and 41 pixels.

resulting in differing from the physical phantom, which a small inhomogeneity sometimes remains in the so call as a homogeneous phantom, (b) the noise homogeneity is easier to control compared to real images, influenced by many factors, such as beam hardening and artifact, and (c) the magnitude and type of noise can be easily determined and changed as desired [31]. However, the real images of the ACR phantom are evaluated to ensure the dependency between ROI size and noise, in addition to the computational phantom images.

Based on the results, the size of ROI strongly influenced the measured noise with a recommendation of using a minimum ROI size of 21×21 pixels to obtain similar noise values as its ground truth. This study only evaluated the noise level up to 100 HU in favor of being widely used in clinical practices [19, 21, 35]. Noise fluctuation using ROI sizes below 21×21 pixels happens because of a too-small ROI size, which cannot capture the random events of the pixel values. Therefore, ROI sizes below 21×21 pixels produce an inaccurate noise result greater than $\pm 5\%$ noise variation from its ground truth value.

These findings confirmed that the recommendation from AAPM, i.e. the ROI size must be at least 1% of the image area [29], is robust enough to detect noise. Since the CT clinical images generally have pixels of 512×512 , 1% of that number of pixels are around 2,621 or about 51×51 pixels, which is much larger than 21×21 pixels.

However, noise measurements with a minimum ROI size of 21×21 pixels produce accurate measurable noises, noise characterization by using SD value only indicates the level of noise without any explanation of the type of noise and image texture. Therefore, accompanying the analysis with histogram curve evaluation and noise power spectrum (NPS) is used to find the type of noise and its image texture, respectively [25,26]. Besides, noise measurement by using its SD is only valid for a uniform noise. Whereas at present, most noise

in modern CT images is non-uniform due to the use of an iterative reconstruction method [36] or non-linear filters [37]. It is known that denoising can occur aggressively in homogeneous regions and less aggressively in heterogeneous regions, such as a bilateral filter [38], or non-local mean filter [39]. However, until now, noise characterization for non-uniform noise is still under development. Some metrics for characterizing non-uniform noise are the noise non-uniformity index [29] and the noise inhomogeneity index (η) [29].

Conclusion

The ROI size was evaluated for accurate noise measurement using homogeneous computational and ACR phantoms. The Gaussian noise with various noise levels of 5, 10, 25, 50, 75, and 100 HU were added to the homogeneous computational phantom. The ACR phantom was scanned with different slice thicknesses of 1.5, 3, 5, and 7 mm to obtain noise variation. The noises were then measured using ROIs with various sizes from 3×3 up to 41×41 pixels. A minimum ROI size is required to maintain the accuracy of noise measurement. A minimum ROI size of 21×21 pixels is needed to obtain similar noise levels as its ground truth. These results were obtained using either computational phantom or using phantom ACR for various noise levels.

Authors' Contribution

Ch. Anam, WS. Budi, and Z. Muhlisin designed the project. A. Naufal, Z. Arifin, and E. Setiawati performed the experiments. Ch. Anam and A. Naufal made the computational phantom. All the authors read, modified, and approved the final version of the manuscript.

Ethical Approval

The research was approved by the Institutional Ethical Committee of Diponegoro University.

Funding

This work was funded by the World Class Research University (WCRU), Diponegoro Univer-

sity, No. 118-08/ UN7.6.1/PP/2021.

Conflict of Interest

None

References

- Solomon JB, Li X, Samei E. Relating noise to image quality indicators in CT examinations with tube current modulation. *AJR Am J Roentgenol*. 2013;**200**(3):592-600. doi: 10.2214/AJR.12.8580. PubMed PMID: 23436849.
- Nowik P, Bujilla R, Poludniowski G, Fransson A. Quality control of CT systems by automated monitoring of key performance indicators: a two-year study. *J Appl Clin Med Phys*. 2015;**16**(4):254-65. doi: 10.1120/jacmp.v16i4.5469. PubMed PMID: 26219012. PubMed PMCID: PMC5690007.
- Schuhbaeck A, Schaefer M, Marwan M, Gauss S, et al. Patient-specific predictors of image noise in coronary CT angiography. *J Cardiovasc Comput Tomogr*. 2013;**7**(1):39-45. doi: 10.1016/j.jcct.2012.10.011. PubMed PMID: 23352772.
- Melnyk R, DiBianca FA. Modeling and measurement of the detector presampling MTF of a variable resolution x-ray CT scanner. *Med Phys*. 2007;**34**(3):1062-75. doi: 10.1118/1.2436977. PubMed PMID: 17369872. PubMed PMCID: PMC1828124.
- Anam C, Fujibuchi T, Budi WS, Haryanto F, Dougherty G. An algorithm for automated modulation transfer function measurement using an edge of a PMMA phantom: Impact of field of view on spatial resolution of CT images. *J Appl Clin Med Phys*. 2018;**19**(6):244-52. doi: 10.1002/acm2.12476. PubMed PMID: 30338920. PubMed PMCID: PMC6236841.
- Anam C, Fujibuchi T, Haryanto F, Budi WS, Sutanto H, et al. Automated MTF measurement in CT images with a simple wire phantom. *Polish Journal of Medical Physics and Engineering*. 2019;**25**(3):179-87. doi: 10.2478/pjmpe-2019-0024.
- Bellesi L, Wyttenbach R, Gaudino D, Colleoni P, et al. A simple method for low-contrast detectability, image quality and dose optimisation with CT iterative reconstruction algorithms and model observers. *Eur Radiol Exp*. 2017;**1**(1):18. doi: 10.1186/s41747-017-0023-4. PubMed PMID: 29708194. PubMed PMCID: PMC5909349.
- Anam C, Haryanto F, Widita R, Arif I. New noise reduction method for reducing CT scan dose: combining Wiener filtering and edge detection algorithm. *AIP Conf Proc*. 2015;**1677**(1):040004. doi: 10.1063/1.4930648.
- Zhou Y, Scott A, Allahverdian J, Lee C, et al. On the relationship of minimum detectable contrast to dose and lesion size in abdominal CT. *Phys Med Biol*. 2015;**60**(19):7671-94. doi: 10.1088/0031-9155/60/19/7671. PubMed PMID: 26389637.
- Viry A, Aberle C, Racine D, Knebel JF, Schindera ST, et al. Effects of various generations of iterative CT reconstruction algorithms on low-contrast detectability as a function of the effective abdominal diameter: A quantitative task-based phantom study. *Phys Med*. 2018;**48**:111-8. doi: 10.1016/j.ejmp.2018.04.006. PubMed PMID: 29728223.
- González-López A. Effect of noise on MTF calculations using different phantoms. *Med Phys*. 2018;**45**(5):1889-98. doi: 10.1002/mp.12847. PubMed PMID: 29500817.
- Mori I, Machida Y. Deriving the modulation transfer function of CT from extremely noisy edge profiles. *Radiol Phys Technol*. 2009;**2**(1):22-32. doi: 10.1007/s12194-008-0039-9. PubMed PMID: 20821125.
- Hsieh J. Computed Tomography: Principles, Design, Artifacts, and Recent Advances. SPIE Press; 2009. Chapter 5.
- Verdun FR, Racine D, Ott JG, Tapiovaara MJ, Toroi P, Bochud FO, Veldkamp WJH, Schegerer A, Bouwman RW, Giron IH, Marshall NW, Edyvean S. Image quality in CT: From physical measurements to model observers. *Phys Med*. 2015;**31**(8):823-43. doi: 10.1016/j.ejmp.2015.08.007. PubMed PMID: 26459319.
- Wu P, Stayman JW, Sisniega A, Zbijewski W, et al. Statistical weights for model-based reconstruction in cone-beam CT with electronic noise and dual-gain detector readout. *Phys Med Biol*. 2018;**63**(24):245018. doi: 10.1088/1361-6560/aaf0b4. PubMed PMID: 30524041.
- Brady SL, Yee BS, Kaufman RA. Characterization of adaptive statistical iterative reconstruction algorithm for dose reduction in CT: A pediatric oncology perspective. *Med Phys*. 2012;**39**(9):5520-31. doi: 10.1118/1.4745563. PubMed PMID: 22957619.
- Kim M, Lee JM, Yoon JH, Son H, et al. Adaptive iterative dose reduction algorithm in CT: effect on image quality compared with filtered back projection in body phantoms of different sizes. *Korean J Radiol*. 2014;**15**(2):195-204. doi: 10.3348/kjr.2014.15.2.195. PubMed PMID: 24644409. PubMed PMCID: PMC3955785.
- Anam C, Haryanto F, Widita R, Arif I, Dougherty G. An investigation of spatial resolution and noise in reconstructed CT images using iterative reconstruction (IR) and filtered back-projection (FBP). *J Phys: Conf Series*. 2019;**1127**(1):012016. doi: 10.1088/1742-6596/1127/1/012016.

19. Rolstadaas L, Wasbø E. Variations in MTF and NPS between CT scanners with two different IR algorithms and detectors. *Biomed Phys Eng Express*. 2018;**4**(2):025009. doi: 10.1088/2057-1976/aa99ea.
20. McCann C, Alasti H. Comparative evaluation of image quality from three CT simulation scanners. *J Appl Clin Med Phys*. 2004;**5**(4):55-70. doi: 10.1120/jacmp.v5i4.1978. PubMed PMID: 15738921. PubMed PMCID: PMC5723516.
21. Anam C, Budi WS, Adi K, Sutanto H, et al. Assessment of patient dose and noise level of clinical CT images: automated measurements. *J Radiol Prot*. 2019;**39**(3):783-93. doi: 10.1088/1361-6498/ab23cc. PubMed PMID: 31117064.
22. Brunner CC, Stern SH, Minniti R, Parry MI, Skopec M, Chakrabarti K. CT head-scan dosimetry in an anthropomorphic phantom and associated measurement of ACR accreditation-phantom imaging metrics under clinically representative scan conditions. *Med Phys*. 2013;**40**(8):081917. doi: 10.1118/1.4815964. PubMed PMID: 23927331.
23. Husby E, Svendsen ED, Andersen HK, Martinsen ACT. 100 days with scans of the same Catphan phantom on the same CT scanner. *J Appl Clin Med Phys*. 2017;**18**(6):224-31. doi: 10.1002/acm2.12186. PubMed PMID: 28921910. PubMed PMCID: PMC5689914.
24. Christe A, Heverhagen J, Ozdoba C, Weisstanner C, Ulzheimer S, Ebner L. CT dose and image quality in the last three scanner generations. *World J Radiol*. 2013;**5**(11):421-9. doi: 10.4329/wjr.v5.i11.421. PubMed PMID: 24349646. PubMed PMCID: PMC3856334.
25. Kijewski MF, Judy PF. The noise power spectrum of CT images. *Phys Med Biol*. 1987;**32**(5):565-75. doi: 10.1088/0031-9155/32/5/003. PubMed PMID: 3588670.
26. Nakahara S, Tachibana M, Watanabe Y. One-year analysis of Elekta CBCT image quality using NPS and MTF. *J Appl Clin Med Phys*. 2016;**17**(3):211-22. doi: 10.1120/jacmp.v17i3.6047. PubMed PMID: 27167279. PubMed PMCID: PMC5690923.
27. Dolly S, Chen HC, Anastasio M, Mutic S, Li H. Practical considerations for noise power spectra estimation for clinical CT scanners. *J Appl Clin Med Phys*. 2016;**17**(3):392-407. doi: 10.1120/jacmp.v17i3.5841. PubMed PMID: 27167257. PubMed PMCID: PMC5690921.
28. AAPM. Specification and acceptance testing of computed tomography scanners. AAPM REPORT NO. 39; New York: AAPM; 1993.
29. Samei E, Bakalyar D, Boedeker KL, Brady S, Fan J, et al. Performance evaluation of computed tomography systems: Summary of AAPM Task Group 233. *Med Phys*. 2019;**46**(11):e735-56. doi: 10.1002/mp.13763. PubMed PMID: 31408540.
30. Dougherty G, Kawaf Z. The point spread function revisited: image restoration using 2-D deconvolution. *Radiography*. 2001;**7**(4):255-62. doi: 10.1053/radi.2001.0341.
31. Gravel P, Beaudoin G, De Guise JA. A method for modeling noise in medical images. *IEEE Trans Med Imaging*. 2004;**23**(10):1221-32. doi: 10.1109/TMI.2004.832656. PubMed PMID: 15493690.
32. Al-Kadi OS. Assessment of texture measures susceptibility to noise in conventional and contrast enhanced computed tomography lung tumour images. *Comput Med Imaging Graph*. 2010;**34**(6):494-503. doi: 10.1016/j.compmedimag.2009.12.011. PubMed PMID: 20060263.
33. Mello-Amoedo CD, Martins AN, Tachibana A, Pinho DF, Baroni RH. Comparison of Radiation Dose and Image Quality of Abdominopelvic CT Using Iterative (AIDR 3D) and Conventional Reconstructions. *AJR Am J Roentgenol*. 2018;**210**(1):127-33. doi: 10.2214/AJR.17.18025. PubMed PMID: 29140117.
34. Bujila R, Fransson A, Poludniowski G. Practical approaches to approximating MTF and NPS in CT with an example application to task-based observer studies. *Phys Med*. 2017;**33**:16-25. doi: 10.1016/j.ejmp.2016.10.016. PubMed PMID: 28003136.
35. Assi AA, Arra AA. Optimization of image quality in pulmonary CT angiography with low dose of contrast material. *Polish Journal of Medical Physics and Engineering*. 2017;**23**(2):43-6. doi: 10.1515/pjmpe-2017-0008.
36. Hussain FA, Mail N, Shamy AM, Suliman A, Saoudi A. A qualitative and quantitative analysis of radiation dose and image quality of computed tomography images using adaptive statistical iterative reconstruction. *J Appl Clin Med Phys*. 2016;**17**(3):419-32. doi: 10.1120/jacmp.v17i3.5903. PubMed PMID: 27167261. PubMed PMCID: PMC5690909.
37. Hilts M, Jirasek A. Adaptive mean filtering for noise reduction in CT polymer gel dosimetry. *Med Phys*. 2008;**35**(1):344-55. doi: 10.1118/1.2818742. PubMed PMID: 18293589.
38. Al-Hinnawi AR, Daear M, Huwajjah S. Assessment of bilateral filter on 1/2-dose chest-pelvis CT views. *Radiol Phys Technol*. 2013;**6**(2):385-98. doi: 10.1007/s12194-013-0212-7. PubMed PMID: 23605697.
39. Li Z, Yu L, Trzasko JD, Lake DS, Blezek DJ, et al. Adaptive nonlocal means filtering based on local noise level for CT denoising. *Med Phys*. 2014;**41**(1):011908. doi: 10.1118/1.4851635. PubMed PMID: 24387516.